Vortex Imaging in Unconventional Superconductors

S.J.Bending[a*], P.J. Curran[a], W.M.A. Desoky[a], V.V. Khotkevych[a,b], A. Gibbs[b], A.P. Mackenzie[b], T. Tamegai[c] & S.E. Sebastian[d]

[a]*Department of Physics, University of Bath, Claverton Down, Bath BA2 7AY, UK*

[b]*School of Physics and Astronomy, University of St Andrews, St Andrews KY16 9SS, UK*

[c]*Department of Applied Physics, University of Tokyo, Tokyo 113-8627, Japan*

[d]*Cavendish Laboratory, University of Cambridge, Cambridge CB3 0HE, UK*

Elsevier use only: Received date here; revised date here; accepted date here

Abstract

The real space imaging of vortices in unconventional superconductors not only provides important information about the effectiveness of flux pinning that can inform high current applications, but also yields crucial insights into the form of the superconducting order parameter. For example, the structure of the vortex lattice reflects effective mass and order parameter anisotropies within the material, and profiles of isolated vortices provide a local measure of the magnetic penetration depth that can be used to infer the superfluid density. We describe here the analysis of recent studies whereby state-of-the-art scanning Hall probe microscopy (SHPM) has been used to perform vortex-resolved magnetic imaging on two distinct families of unconventional superconductors. Two sets of results will be analysed in detail; (i) vortex lattice structural transitions in the p-wave superconductor Sr_2RuO_4 that reflect underlying anisotropies in the system and (ii) a quantitative analysis of vortex profiles in Co-doped 122 pnictide superconductors ($SrFe_{2-x}Co_xAs_2$ & $BaFe_{2-x}Co_xAs_2$) that allows one to infer the temperature-dependent superfluid density. The latter has then been compared with predictions for different order parameter models for a multiband superconductor.

Keywords: Type your keywords here, separated by semicolons ;
PACS: Type your PACS codes here, separated by semicolons ;

* Corresponding author. Tel.: +44 1225 386173; fax: +44 1225 386110; e-mail: pyssb@bath.ac.uk.

1. Introduction

Real space vortex imaging is a powerful investigative probe for novel unconventional type II superconducting materials. The spatial symmetry of vortex structures reflects underlying electronic and order parameter anisotropies [1]. Magnetic imaging also allows one to search directly for spontaneous currents/fields due to time reversal symmetry breaking (TRSB) [2]. In addition 'local' penetration depth (superfluid density) measurements yield information about the number of gapped bands contributing to superconductivity as well as the symmetry of the order parameter associated with each of these [3].

Here we illustrate how high resolution scanning Hall probe microscopy can be used to image discrete vortices in the p-wave superconductor Sr_2RuO_4. The symmetry of the vortex lattice reveals important information about intrinsic electronic and superconducting anisotropies in this material. In the case of Co-doped 122 Fe-pnictide single crystals a detailed analysis of the temperature dependence of the penetration depth of individual vortices gives strong evidence for the presence of two gaps, and indications for the symmetry of the order parameter of these.

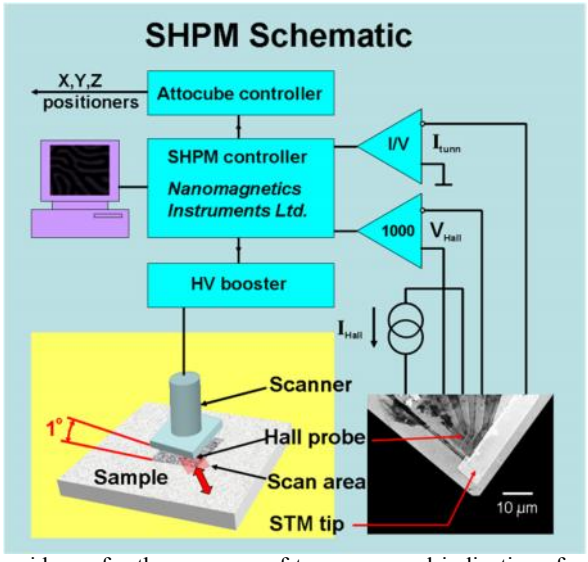

Fig. 1 (colour online) Schematic diagram of a typical SHPM system with STM-tracking.

2. Experimental Method; Vortex Imaging

High resolution scanning Hall probe microscopy (SHPM) has been used to perform the local magnetic imaging presented here. SHPM is a non-invasive magnetic imaging technique whereby a sub-micron Hall effect sensor is scanned just above the surface of the sample to be imaged in order to generate two-dimensional maps of the local magnetic induction. Fig. 1 shows a schematic of our microscope which is a modified low temperature STM in which the usual tunnelling tip at the end of the piezoelectric scanner tube has been replaced by a microfabricated GaAs/AlGaAs heterostructure chip. Electron beam lithography and wet chemical etching were used to define a sub-micron (typically 0.6 - 0.8 μm) Hall probe in the two-dimensional electron gas approximately 5 μm from the corner of a deep mesa etch, which was coated with a thin Au layer to act as in integrated STM tip. The sample sits on an inertial motor and is first approached towards the sensor until tunnelling is established and then retracted about 100-200 nm allowing rapid scanning. The Hall probe makes an angle of about 1° with the sample plane so that the STM tip is always the closest point to the surface, and each 2D map of magnetic induction is usually divided into 128×128 pixels. If required, several images (~10) are averaged frame-by-frame to suppress low frequency noise arising from the Hall sensor. High temperature measurements (T>4.5K) of pnictide single crystals were performed with a commercial SHPM system manufactured by Nanomagnetic Instruments Ltd [4] with a scan range of ~8μm×8μm at 5K. Investigations of low T_c single crystals of Sr_2RuO_4 were performed on a custom-built scanner head that mounts directly onto the cold plate of an Oxford Heliox He^3-refrigerator, allowing measurements down to ~300mK with a larger field of view of 14μm×14μm [5]. Although the spatial resolution of SHPM is only modest, being limited by a combination of the geometrical Hall sensor size and the sample/sensor spacing, it does have a number of advantages over other magnetic imaging techniques. It can be used over a very broad range of temperatures in the presence of large external magnetic fields, and produces a quantitative measure of one component of the local magnetic induction, B_z.

Fig. 2 (colour online) SHPM images of vortices in a Sr_2RuO_4 single crystal at T=300mK after field-cooling in the indicated magnetic fields (scan size ~14μm×14μm). (d) A model fit to a vortex profile at H=0.2Oe.

3. Experimental Results

3.1. Sr_2RuO_4 Single Crystals

Superconducting Sr_2RuO_4 single crystals were grown using the floating-zone technique with Ru self-flux in a commercial image furnace [6] and annealed in air (1500°C for 3 days) to remove lattice defects and reduce vortex pinning [7]. Here we present results on a very high quality sample with a very sharp transition at T_c=1.5K, as measured by ac susceptibility. There is no detectable sign of any additional phases, and de Haas-van Alphen measurements indicate very long carrier mean free paths (~1μm).

Fig. 2 shows a family of SHPM images captured parallel to the a-b crystal face, after field cooling to

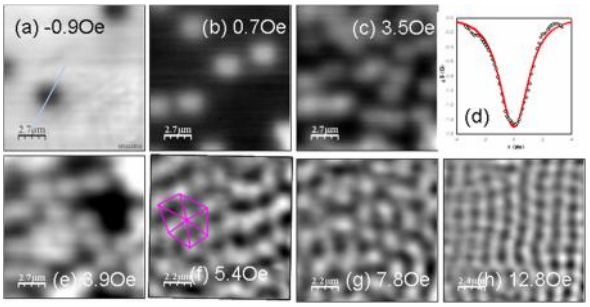

T~300mK from above T_c (H // c-axis) in various cooling fields. Fig. 2(d) shows a fit to the profile across a well-isolated vortex measured at H=0.2 Oe (c.f., Fig. 2(a)) based on the Clem variational model [8], modified to account for surface screening effects using an approach due to Kirtley *et al.* [9], assuming a variational coherence length ξv=66nm, λ=165nm and an active Hall probe width, w, of 600nm. Although at first sight the fit seems good, and confirms that the vortex contains a superconducting flux quantum, we have had to input an unrealistically large scan height of z=1.26μm (based on other measurements we believe z~0.8μm), suggesting that there is some unexplained vortex broadening that is not accounted for in our model. In addition, a careful statistical analysis of vortex-vortex spacings after Delaunay triangulation at intermediate fields (c.f., Fig. 2(c)) reveals no evidence for vortex coalescence that has recently been proposed to arise from a weak long range vortex attraction at low fields [2,10].

As we increase the applied field (H // c-axis) above 4Oe we witness the emergence of first triangular and then square vortex order out of the essentially random low field distributions as illustrated in Figs. 2(e)-(h). Fig. 2(e) at 3.9Oe shows a rather random distribution of weakly pinned vortices. However, upon increasing the field to just 5.4Oe (Fig. 2(f)) we start to see a pronounced degree of triangular order as indicated by the hexagonal mesh superimposed on the raw vortex image. This reflects the emergence of the usual triangular Abrikosov vortex lattice driven by vortex-vortex repulsion. Surprisingly the triangular lattice is lost again at 6.8 Oe (Fig. 2(g)) and there appears to be some

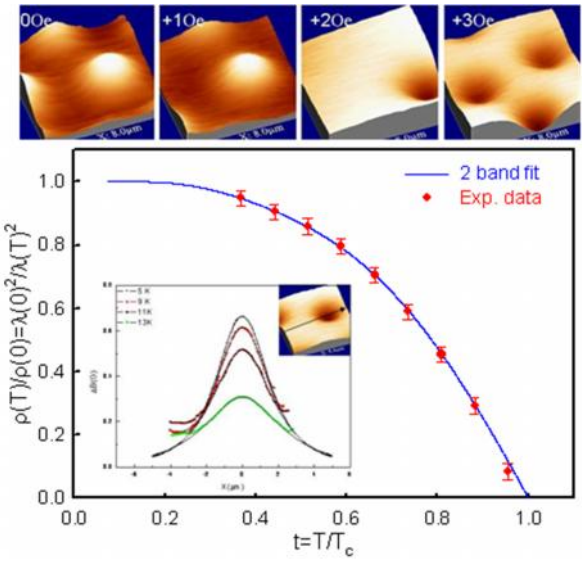

Fig. 3 (colour online) (Top) SHPM images of vortices in a $SrFe_{2-x}Co_xAs_2$ (x~0.11) single crystal at T=8K after field-cooling in the indicated magnetic fields (scan size ~8μm×8μm). (Bottom) Two band model fit to the inferred temperature-dependent superfluid density (see text). Inset illustrates model fits to the vortex profile at a few selected temperatures.

competition between two different forms of order. Indeed for yet higher applied fields we find a transition to a square vortex lattice, which is almost complete in the rather well-ordered image shown at 12.7 Oe (Fig. 2(h)). The formation of a square vortex lattice is in agreement with earlier neutron diffraction [11] and muon [12] data. Within the resolution of our experiment we find that the lattice spacing in both x- and y-scan directions is the same, ruling out rectangular ordering in fields up until 35.3 Oe. Using an extended London theory approach theory (κ>>1) for a two component p-wave order parameter, Heeb and Agterberg [13] have investigated the ground state vortex structure in Sr_2RuO_4 as a function of Fermi surface anisotropy, $|\nu|$ << 1, and applied field. They predict a continuous triangular → rectangular → square field-driven transition, with switching fields that are strongly dependent on the value of ν. Since the extended London theory assumes that κ>>1 it does not strictly apply to Sr_2RuO_4 (κ≈2.5), and we are unable to draw any quantitative conclusions about the magnitude of ν. Our observed crossover is at considerably lower fields than in the high κ (κ=5, κ=25) simulations of Heeb and Agterberg, but the same authors note that the crossover to a square lattice would occur at lower applied fields and lower anisotropies for a superconductor with smaller κ.

3.2 Co-doped $SrFe_2As_2$ and $BaFe_2As_2$ Single Crystals

We have studied high quality single crystal samples of the Co-doped '122' superconductors $SrFe_{2-x}Co_xAs_2$ prepared by the flux growth technique [14] and $BaFe_{2-}$

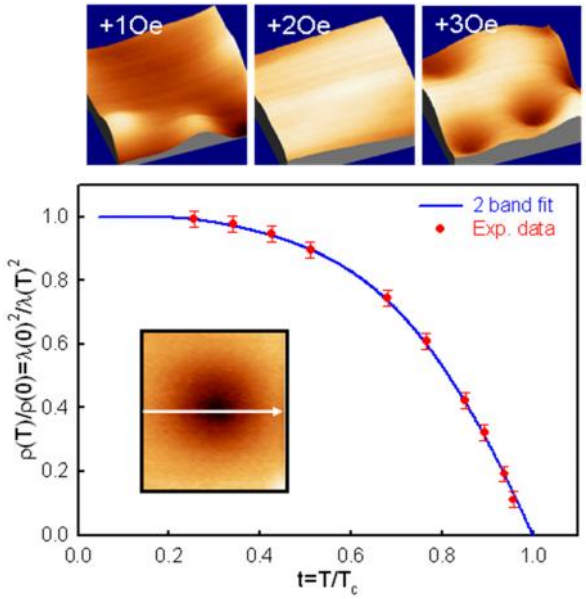

Fig. 4 (colour online) (Top) SHPM images of vortices in a $BaFe_{2-x}Co_xAs_2$ (x~0.075) single crystal at T=12K after field-cooling in the indicated magnetic fields (scan size ~8μm×8μm). (Bottom) Two band model fit to the inferred temperature-dependent superfluid density.

$_xCo_xAs_2$ prepared by the self-flux method [15] using high purity starting elements (>99.99%).

Fig. 3 (top) shows a set of vortex images captured on a $SrFe_{2-x}Co_xAs_2$ (x~0.11) single crystal after field-cooling to T=8K from $T>T_c$ in very small perpendicular applied magnetic fields (in addition to the earth's field ~ +1.3Oe). The onset of a diamagnetic signal in 'local' magnetisation loops with the Hall sensor positioned just above the sample surface indicated that T_c=13.65±0.05K, in good agreement with independent measurements on otherwise identical crystals. At 8K the temperature-dependent scan range of the piezoelectric tube is ~8μm×8μm and, in the absence of any diamagnetic screening, we would expect to generate about 3 vortices per Oersted on average. In practice, although changes in number and sign of vortices as a function of field are qualitatively what one would expect, the actual number of vortices seen is considerably less than this estimate indicating quite strong magnetic screening. In addition we have studied the temperature dependence of several well-isolated vortices at fixed magnetic field. The inset of Fig. 3 (bottom) shows one particular example after field-cooling at H=+1Oe. Vortex profiles at each temperature have been fitted to a variational model due to Clem [8], modified to account for surface screening effects using an approach due to Kirtley *et al.* [9], assuming a variational coherence length ξ_v=2.5nm, an active Hall probe width, w, of 800nm and a temperature-dependent penetration depth. Following a procedure described by Luan *et al*. [16] to describe MFM force curves we use the results of these fits to calculate the superfluid density, $\rho_s(T)/\rho_s(0)=\lambda(0)^2/\lambda(T)^2$, which is then fit to a two band model with two full gaps. This model assumes that $\rho_s(T)=p\rho_1(T)+(1-p)\rho_2(T)$, where $\rho_{1,2}(T)$ are the superfluid densities in the two different bands and p takes account the relative contribution from each. The individual superfluid densities have been calculated assuming the following expression for isotropic s-wave pairing [3]

$$\rho_i(T) = 1 - \frac{1}{2kT}\int_0^\infty \cosh^{-2}\left(\frac{\sqrt{\varepsilon^2+\Delta_i(T)^2}}{2kT}\right)d\varepsilon. \qquad (1)$$

Here the gap was assumed to be given by

$$\Delta_i(T) = \Delta_i(0)\tanh\left[\frac{\pi kT_c}{\Delta_i(0)}\sqrt{a_i\left(\frac{T_c}{T}-1\right)}\right], \qquad (2)$$

where a_i is a characteristic parameter that reflects the specific pairing state (a_i=1 for isotropic s-wave pairing). Fig. 3 (bottom) shows the experimentally measured dependence of the superfluid density along with the fits to our two-gap model with Δ_1=4.80kT_c, Δ_2=2.00kT_c, p=0.49, and a_1=0.94, a_2=1. Gap values for the two bands were estimated from prior point contact spectroscopy measurements [17] and the values of a_i and x were extracted from a numerical fitting programme. It is generally assumed that the smaller gap is located on the hole pocket at the Γ-point, and we see that in this case the superfluid density appears to be fairly equally shared between these hole pockets and electron pockets at the M-points. Making the usual assumption that the hole gap is isotropic s-wave (a_2=1), our fitted value of a_1=0.94 is rather close to unity within our experimental errors indicating that the electron gap is also close to isotropic s-wave with no clear evidence for nodes.

Fig. 4 shows comparable data for a $BaFe_{2-x}Co_xAs_2$ single crystal close to optimal doping (x=0.075, T_c=23.3K). Fig. 4 (top) shows a set of images obtained after field cooling in small applied fields to T=12K from $T>T_c$. Fig. 4 (bottom) shows the temperature dependence of the superfluid density calculated from fits of λ(T) to well isolated vortices as discussed above. This is well described by our two gap model with Δ_1=3.3kT_c, Δ_2=1.3kT_c, p=0.76, and a_1=1.92, a_2=1, very similar to the fit parameters obtained from the MFM measurements of Luan *et al*. [18] for a sample with a similar T_c. The much larger value for a_1 for this Ba sample suggests that the electron gap in this material is probably not isotropic s-wave, and gap nodes cannot be ruled out.

4. Conclusions

Direct vortex imaging has been used to gain insights into the nature of superconductivity in a range of unconventional superconductors. We find no evidence of

vortex clustering in very highly ordered Sr_2RuO_4 single crystal samples at low fields, but the field profiles of isolated vortices do reveal an unidentified source of broadening. We have resolved a field-driven triangular (H<7Oe) → square (H>7Oe) vortex lattice transition in our highest ordered samples at low fields, consistent with extended London theory calculations for a p-wave order parameter. We have fitted the temperature dependent vortex profiles in Co-doped 122 Fe-pnictide superconductors to extract the temperature dependence of the superfluid density. For both $SrFe_{2-x}Co_xAs$ (x=0.11) and $BaFe_{2-x}Co_xAs$ (x=0.075) ρ(T) fits well to a two band model with two full gaps. Our fit parameters suggest that the larger gap for the Sr sample is close to isotropic s-wave, while the symmetry of the order parameter corresponding to the larger gap in the Ba sample is almost certainly anisotropic and could possibly contain nodes.

5. Acknowledgements

This work was supported by the Engineering and Physical Sciences Research Council (EPSRC) in the U.K. under grants number EP/D034264/1 and EP/E039944/1.

References

[1] M.H.S. Amin et al., Phys. Rev. B 58, 5848 (1998),
[2] V. O. Dolocan *et al.*, Phys Rev Lett **95**, 097004 (2005); J.R. Kirtley *et al.*, Phys Rev B **76**, 014526 (2007); C.W. Hicks *et al*., Phys Rev B **81**, 214501 (2010); P.G. Bjornsson *et al*., Phys Rev B **72**, 012504 (2005).
[3] Ruslan Prozorov *et al*., Supercond. Sci. Technol. **19**, R41 (2006).
[4] http://www.nanomagnetics-inst.com/.
[5] V.V. Khotkevych *et al*., Rev Sci Instrum **79**, 123708 (2008).
[6] Y. Maeno *et al*., Journal of low temperature physics **105**, 1577 (1996).
[7] Z. Q. Mao *et al*., Materials Research Bulletin **35**, 1813 (2000).
[8] J. Clem, Journal of low temperature physics **18**, 427 (1975).
[9] J.R. Kirtley *et al*., Rev. B **76**, 014526 (2007).
[10] K. Hasselbach *et al*., Physica C-Superconductivity and Its Applications **460**, 277 (2007).
[11] T.M. Riseman *et al.*, Nature **404**, 629 (2000).
[12] G.M. Luke *et al*., Physica B: Condensed Matter **289-290**, 373 (2000).
[13] R. Heeb and D. F. Agterberg, Physical Review B **59**, 7076 (1999).
[14] P.Alireza P et al., J. Phys.: Condens. Matter **21**, 012208 (2009)
[15] Y. Nakajima, T. Taen and T. Tamegai, J. Phys. Soc. Jpn. **78**, 023702 (2009).
[16] Lan Luan *et al*., PRB **81**, 100501(R) (2010).
[17] C.R. Hunt *et al*., Abstract: X23.00013, Bulletin of the American Physical Society, APS March Meeting 2011, Volume **56**, Number 1, March 21–25, 2011; Dallas, Texas
[18] Lan Luan, PhD Thesis, Magnetic Force Microscopy Studies of Unconventional Superconductors; Single Vortex Manipulation and Magnetic Penetration Depth Measurement, Stanford University, March 2011.